A comparison among wide bandgap devices using a CLLLC bidirectional resonant converter

Alejandro Llop[1], Kepa Mendibil[1], Íñigo Peña[1], Salvador Ceballos[1], Susana Apiñániz[1]

[1] Tecnalia, Basque Research and Technology Alliance (BRTA), Derio, Spain.

Corresponding author: Alejandro Llop, alejandro.llop@tecnalia.com

Abstract

In this paper, the design of a 6.6 kW 500 kHz CLLLC bidirectional resonant converter platform is presented, which has been used to compare wide bandgap semiconductors of different technologies: GaN with cascode structure and SiC. The platform, designed by simply changing the gate driver board in it, permits rapidly changing from GaN to SiC and vice versa. The converter is able to operate with an input voltage of 380–600 V, an output voltage of 280-450 V and a maximum power of 6.6 kW, using a frequency operating range of approximately 300-700 kHz, which, along with the resonant behaviour of the converter, allows very high power density and reduction of the passive components. In addition, synchronous rectification is implemented in the secondary, achieving a compact design. Several measurements have been conducted using the same platform to compare the semiconductors from different technologies using commercial discrete devices for several frequencies in different operation modes (below, at, and above resonant frequency). Efficiency, switching times and their waveforms and the influence of gate resistors on the commutation process have been the figures selected to benchmark the semiconductor technologies.

1 Introduction

The estimated increase in energy used in transportation is around 44% by 2035, compared to 2008 [1]. In order to reduce carbon emissions and the consumption of fossil fuels, electrified vehicles are born. This type of vehicle stores the charge in rechargeable batteries, which is why both battery chargers and a recharging infrastructure are necessary. Electric vehicles can be recharged in residential or public areas; in the literature, three types of chargers are described depending on the type of charge:

- Level 1: slow charging from domestic charging points (single phase) of 230 V and up to 20 A (EU).
- Level 2: slow charging from private or public charging points (single-phase or three-phase) of 400 V and up to 32 A (EU).
- Level 3: fast charging from a special charging station (three-phase) of 480 V and with a power greater than 50 kW [2].

Due to the development of bi-directional power conversion technologies, electric vehicles (whether plug-in hybrids or fully electric) are capable of not only consume power from the electrical grid, but also supply the energy stored in their batteries to the grid. In this way, electric vehicles can behave as loads or as generators for the network, increasing the efficiency and reliability of the distribution network. According to current literature [3], for this feature to have a positive impact on the network, the appropriate hardware, intelligent connections to the network, and control of interactive charging hardware must be available. This way, electric vehicles can serve as versatile energy storage resources, providing vehicle-to-grid (V2G) services, as a way to endow the grid with greater flexibility, efficiency and reliability.

Bidirectional electric vehicle chargers play a crucial role for the development of all these functionalities. This paper analyses a level 2 DC-DC bidirectional power converter, which could be present in an architecture like the one in Fig. 1. Besides, to increase the efficiency and power density one step further, the adoption of a resonant topology along with the use of wide bandgap devices is considered.

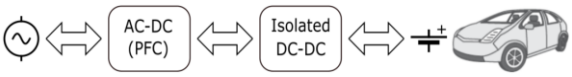

Fig. 1 One common architecture of bidirectional On Board Chargers

Wide bandgap devices can lead to the development of more compact and efficient power converters, due to their better features compared to silicon as higher operating temperature and voltage and reduction of losses, which allows to rise the switching frequency and hence the reduction of passive components. However, they also have drawbacks, such as a higher cost and EMI emissions due to their superior dv/dt and di/dt during switching transient, resulting in a commonly known trade-off [4].

Some of these issues can be overcome by using resonant topologies in combination with wide bandgap semiconductors. These paper measures the following improvements when both technologies are combined:

- Turn on losses are practically zero due to zero voltage switching (ZVS).
- Despite of using wide bandgap devices, using a resonant converter allows to minimize EMI emissions compared to a conventional hard-switched converter. Besides, recovery losses due to recovery current are eliminated too, and subsequently the corresponding overshoot in the complementary MOSFET, which leads to a further reduction in EMI.
- Switching and conduction losses are considerably lower compared to silicon.

The present study aims to highlight the differences seen in the practice between GaN cascode [5] and SiC MOSFETs over the same platform with minimal changes, using a resonant converter very much in vogue nowadays, due to its characteristics of efficiency, soft switching, bidirectionality and variable input and output voltage ranges, the CLLLC converter, as shown in Fig. 3.

The rest of the paper is organized as follows:

Section II explains the design of the converter, including the critical parameters and the choice of the circuit components. It also covers succinctly the different operation modes and the type of control implemented.

Section III firstly introduces the evaluation platform developed, briefly indicating its main characteristics. Afterwards, the necessary differences in the circuit to go from testing GaN cascode semiconductors to SiC and vice versa are emphasized.

Section IV shows the experimental results obtained. It accounts for the difference in terms of efficiency, switching times and waveforms when GaN and SiC technologies are evaluated over the same platform while changing the minimum components in the converter circuit. Furthermore, the influence of gate resistor, frequency and power are considered for a more complete study of the main wide bandgap technologies.

2 Design of the resonant converter

The design process of both the unidirectional and bidirectional LLC and CLLLC converters is conveniently detailed in the literature [6]-[12]; it will be briefly explained below for the proper design of the converter object of study in this paper. The converter scheme is illustrated in Fig. 3, whose main parameters and specifications are summarized in Table 1.

$f_{s,range}$ (kHz)	300-700
$f_{s,nom}$ (kHz)	500
$V_{IN,range}$ (V)	380-600
$V_{OUT,range}$ (V)	280-450
$P_{OUT,max}$ (kW)	6.6
L_m (µH)	25
$L_{\sigma p}$ (µH)	1.9
L_n	13
C_p (nF)	57.4
C_s (nF)	82
n_p:n_s	8:6

Table 1 Design specifications and parameters

In order to guarantee the ZVS operation of the primary power switches and a stable control loop, the operation of the converter must remain in the inductive region. Besides, Eq. (1) must be met to achieve ZVS in the turn-on process. The effective value of C_{oss} has been obtained empirically from the manufacturer datasheets using Eq. (2).

$$L_m \leq \frac{t_{dt}}{16 \cdot C_{oss,eff} \cdot f_{s,max}} \quad (1)$$

$$C_{oss,eff} = \frac{1}{V_{DS,max}} \cdot \int_0^{V_{DS,max}} C_{oss}(V_{DS}) \cdot dV_{DS} \quad (2)$$

The ratio of L_m to $L_{\sigma p}$ in Eq. (3) is selected to ensure voltage gain in the resonant tank is enough across the operating range of the converter. Then, from Eq. (4), the value of C_p is obtained.

$$L_n = \frac{L_m}{L_{\sigma p}} \quad (3)$$

$$f_{s,nom} = \frac{1}{2\pi\sqrt{L_{\sigma p} \cdot C_p}} \quad (4)$$

Accordingly, the passive components of the secondary are derived from Eq. (5) and Eq. (6):

$$L_{\sigma s} = \frac{L_{\sigma p}}{\left(n_p : n_s\right)^2} \quad (5)$$

$$f_{s,nom} = \frac{1}{2\pi\sqrt{L_{\sigma s} \cdot C_s}} \quad (6)$$

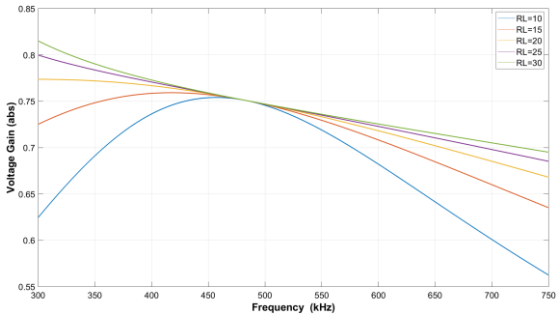

a)

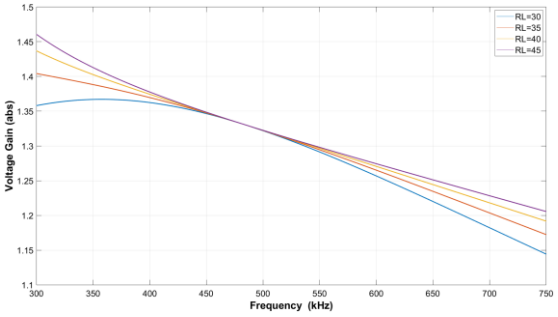

b)

Fig. 2 Voltage gain as a function of switching frequency for L_n = 13 and different loads. a) Direct power flow. b) Reverse power flow

Then, to guarantee that the control is stable along the frequency operating range for both directions of power flow, the magnitude of the voltage gain is represented versus frequency according to First Harmonic Analysis [12] in Fig. 2 and the minimum load resistor is determined in such a way that voltage gain curve is monotonic.

All of the above has been validated by simulation using PLECS.

Properties	**Cree C3M0030090K (SiC)**	**Transphorm TP90H050WS (GaN Cascode)**
Maximum V_{DS} (V)	900	900
Package	TO 247-4	TO 247-3
Maximum V_{GS} (V)	-8/+19	±20
Typ. $R_{DS(on)}$ @ 25ºC (mΩ)	30	50
Typ. $R_{DS(on)}$ @ 150ºC (mΩ)	37	105
Input Capacitance C_{iss} @ V_{DS} 600 V (pF)	1747	1000
Output Capacitance C_{oss} @ V_{DS} 600 V (pF)	131	115
Reverse Transfer Capacitance C_{RSS} @ V_{DS} 600 V (pF)	8	3.5
Diode V_{SD} (V)	4.8 @ 17.5 A	2.2 @ 22 A
Reverse Recovery Q_{rr} (nC)	545 (35 A, 600 V, di/dt 2680 A/µs)	156 (22 A, 600 V, di/dt 1000 A/µs)
Typ. $R_{\theta JC}$ (ºC/W)	0.62	1.05

Table 2 Semiconductors used in this work

3 Evaluation Platform

For the quick evaluation of the semiconductor technologies proposed in this work, SiC and GaN with a cascode structure [13], an evaluation platform has been developed, starting initially from one reference design of Texas Instruments [14] and adding some new features to it to increase the measuring range, get better heat dissipation and allow the use of GaN, apart from the initially proposed SiC, provided that the semiconductor package is TO-247.

The main features of the main board and gate drivers are described below.

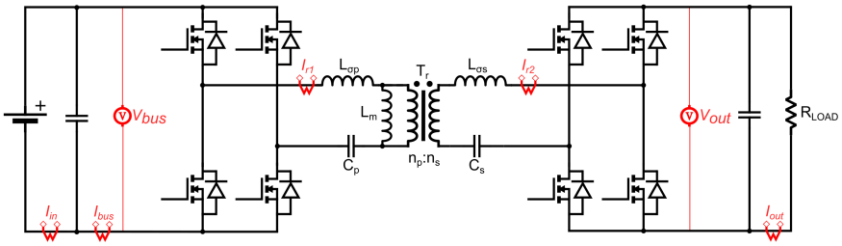

Fig. 3 CLLLC converter including voltage and current measurements in this work

3.1 Main board

It contains the CLLLC power converter represented in Fig. 3, according to the design parameters explained in Section II. Next, its main features are shown in a summarized way:

- Current measurement of the primary (I_{in}, I_{bus}) and secondary dc-sides (I_{out}) and from the resonant tanks (I_{r1}, I_{r2}) to carry out synchronous rectification.
- Voltage measurement of both primary (V_{bus}) and secondary (V_{out}) sides.
- Planar transformer with integrated leakage inductors, with tight tolerances, attached to the heatsink at the bottom to improve its thermal characteristics.
- Overvoltage and overcurrent protections in both primary and secondary.
- Synchronous rectification in both normal and reverse power flow.
- The control board, including the digital signal processor, is referred to the primary, so the measurements from the secondary are galvanically isolated; not so those of the primary.

The main properties of the two semiconductors used in the comparison are summarized in Table 2.

From the parameters of Table 2, it can be summarized that:

- Unlike GaN transistor, SiC has kelvin source (the fourth pin), minimizing the influence of the output power on the input signal.
- SiC transistor has better conduction properties, as reflected by $R_{DS(on)}$. On the contrary, GaN transistor is better in switching, as indicated by the capacitances and reverse recovery.

Finally, regarding the control system, it must process the captured measurements according to the control algorithm to generate the semiconductor on and off signals. This task is especially demanding due to the high switching frequency, thus requiring a high operating speed of the control element. Due to the processing needs and complexity of the control, it has been implemented through a DSP, TMS320F280049C from Texas Instruments. The control has been implemented using frequency modulation, according to [15], [16], and validated experimentally using SFRA libraries [17].

3.2 Gate driver boards

Three different driver boards are designed and assembled to be able to test the semiconductors of Table 2, whose results appear in the next section, and also a hypothetical device of e-mode GaN in TO-247 package. The main difference comes from the supply rails of the drivers used to control the gates: SiC driver board uses (-4 V, 15 V), that of GaN cascode uses (0 V, 15 V) and eventually the GaN gate driver board uses (-4 V, 6 V).

The gate control circuit used after the driver for the eight transistors in the CLLLC with synchronous rectification is that of Fig. 4(a). Nevertheless, to study the influence of gate resistor, which is covered in Section IV, an alternative gate control circuit has also been proposed as shown in Fig. 4(b).

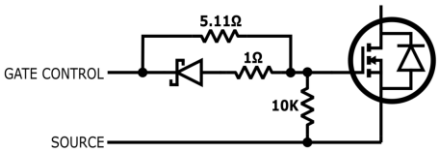

a)

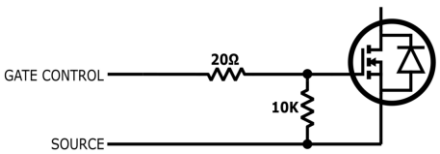

b)

Fig. 4 Gate control circuit after driver. a) Initial values. b) Modified circuit with 20 Ω gate resistor

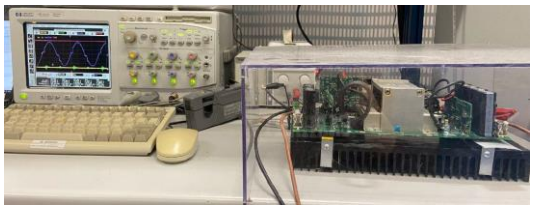

Fig. 5 Setup in the laboratory

4 Experimental results

Using the platform described in Section III and shown in Fig. 5, different tests have been conducted to evaluate and compare the semiconductors mentioned when the CLLLC converter is running in normal mode: power flowing from the input to the output.

Initially, the converter efficiency for two different output voltages is measured depending on the output power and the value of the gate resistor used in the driver. A maximum power level of up to 5 kW has been considered to avoid as much as possible the influence of temperature on losses and operate safely the converter. Three different switching frequencies corresponding to the operating modes of the converter have been considered.

Secondly, the switching waveforms for the different transistors are shown and analysed, so as to see the influence on the previous efficiency measurements.

4.1 Efficiency measurements

These tests have been carried out in open loop, fixing the switching frequency and the output voltage, to analyse the losses of the semiconductors depending on the frequency.

Four cases are represented simultaneously in the following figures: SiC with original gate circuit (Fig. 4(a)), GaN with original gate circuit, SiC with 20 Ω resistor (Fig. 4(b)) and GaN with 20 Ω resistor.

4.1.1 Resonant frequency

In this mode, switching frequency matches resonant frequency of the resonant tank, achieving the highest efficiency [12]. Primary and secondary MOSFETs switch with ZVS and ZCS respectively.

In Fig. 6 it is shown how the efficiency of the power converter varies with the load for the different configurations and two output voltages, V_{OUT} 300 V and 400 V, when switching frequency matches resonant frequency, at approximately 500 kHz. For this frequency, the results obtained with GaN cascode are better than those of SiC, due to the lower switching losses; it is noticeable how for high load, when using 20 Ω gate resistor, the efficiency is improved.

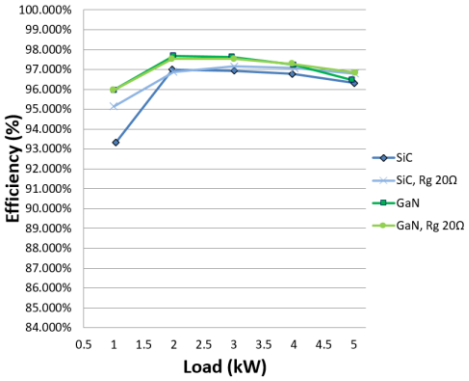

a)

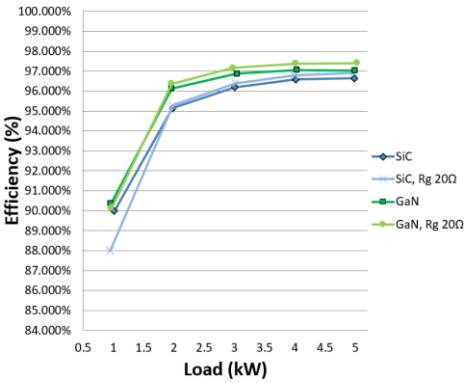

b)

Fig. 6 Converter efficiency as a function of output power at resonant frequency, 500 kHz. a) V_{OUT} = 300 V. b) V_{OUT} = 400 V

4.1.2 Below resonance

When operating below resonance, there is also ZVS for the primary MOSFETs and ZCS for the secondary MOSFETs, since, as stated in [12], operating frequencies below the resonant frequency can guarantee the soft switching of the output rectifiers. However, due to the lower frequency, the discontinuity in the secondary current (DCM: discontinuous conduction mode) causes higher rms currents and hence losses.

In Fig. 7, the efficiency achieved when operating at 375 kHz, i.e. below resonant frequency, is shown. This time, unlike in Fig. 6, the results obtained with SiC are globally better since, at this frequency, the switching losses have less specific weight that the conduction losses in the global efficiency. Since the SiC devices present lower conduction losses, due to their lower $R_{DS(on)}$, than their GaN counterparts, the obtained results are reasonable. When using GaN cascode with 20 Ω gate resistor and high load, some issues have arisen, triggering the converter protections, presumably due to noise.

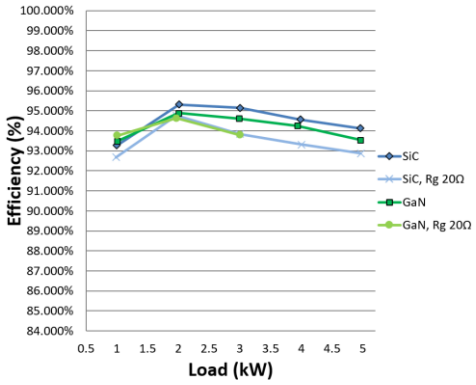

a)

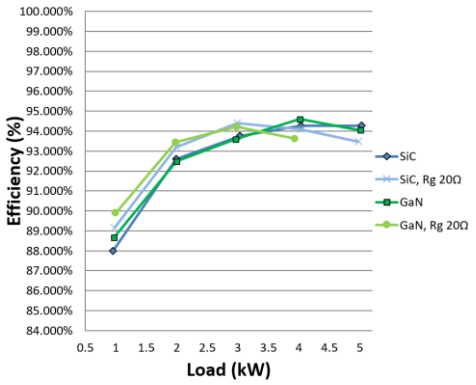

b)

Fig. 7 Converter efficiency as a function of output power below resonance, at 375 kHz. a) V_{OUT} = 300 V. b) V_{OUT} = 400 V

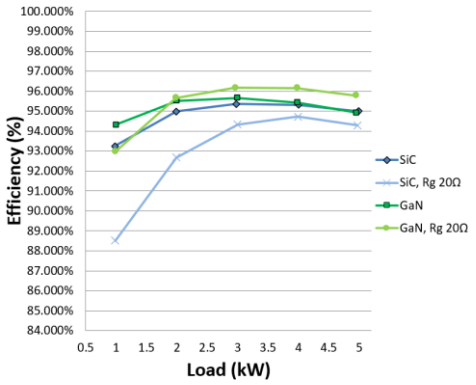

a)

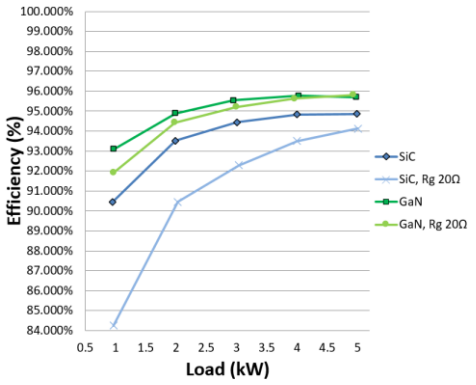

b)

Fig. 8 Converter efficiency as a function of output power above resonance, at 638 kHz. a) V_{OUT} = 300 V. b) V_{OUT} = 400 V

4.1.3 Above resonance

In this mode, the switching frequency is above the series resonant frequency and the magnetizing inductance does not participate in the resonance [18]. Besides, the soft switching of the output synchronous rectifier cannot be achieved, keeping only ZVS for the primary MOSFETs.

In Fig. 8, the efficiency obtained operating above the resonant frequency at 638 kHz is displayed. In this case, the efficiency achieved using GaN cascode devices is remarkably better, accounting for at least one percent efficiency improvement. It is worth noting the low efficiency using SiC with 20 Ω gate resistors; this is because at 638 kHz switching losses are considerable, which are worse in SiC, what is accentuated when switching times are increased due to a higher gate resistor.

4.1.4 Summary

The following conclusions can be derived from the previous results:

- As it is expected, better results are accomplished when switching frequency matches resonant frequency; circulating energy in the resonant network is low.
- At switching frequencies above hundreds of kilohertz, the efficiencies obtained with GaN cascode devices overcome those of SiC.
- In terms of efficiency, the results achieved using 20 Ω gate resistors are comparable to those employing lower gate resistors, except when the switching frequency is below the resonance one; besides, for the higher resistors, the results tend to improve as the load is heavier. In the next section, it will be shown how it affects to the switching waveforms, specially to switching times and undesired effects such as overshoots and ringing.

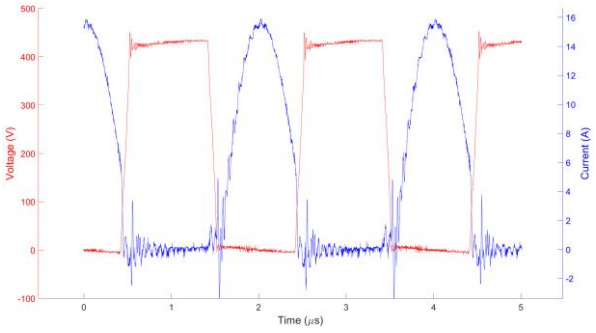

a)

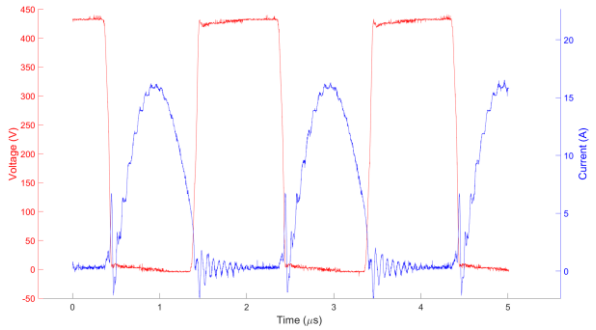

b)

Fig. 9 Switching waveforms for C3M0030090K SiC transistor, 4 kW output power; blue: I_{DS}, red: V_{DS}. a) Original gate circuit. b) Modified circuit with 20 Ω gate resistor

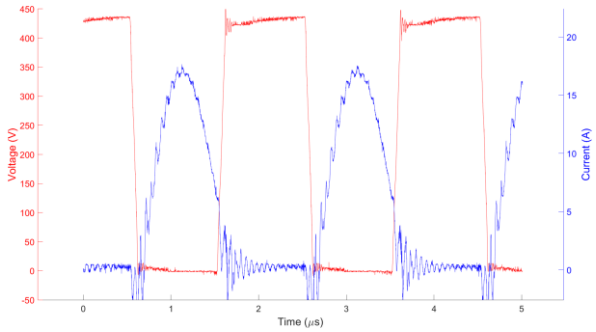

a)

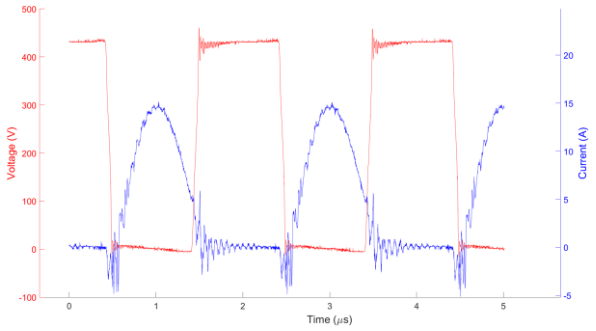

b)

Fig. 10 Switching waveforms for TP90H050WS GaN cascode transistor, 4 kW output power; blue: I_{DS}, red: V_{DS}. a) Original gate circuit. b) Modified circuit with 20 Ω gate resistor

4.2 Switching waveforms

In this section, the waveforms during the turn-on and turn-off switching transients are shown and analysed for one of the primary low-side transistors using the gate control circuits in Fig. 4. Displayed results are obtained when the converter is running at the resonant frequency of the resonant tank and the output power is 4 kW. The same conclusions are valid for operation below and above resonant frequency.

In Fig. 9, the waveforms using SiC are displayed, while Fig. 10 shows those corresponding to GaN cascode transistors.

In order to compare the results, Table 3 summarizes the values obtained for the most interesting metrics, that is, the switching times (measured between 10% and 90% of the final values) and the derivative of the V_{DS} voltage. It is very striking that the switching speeds, both at turn-on and turn-off, increase when the gate resistor is higher; this can explain the best results achieved in the efficiency curves of Fig. 6 at heavy loads when the gate resistor is 20 Ω. This leads to reject the assumption that a higher gate resistor always causes more switching losses and reduces the switching speed, so that a carefully choice of the gate resistor must be carried out by measuring the corresponding efficiencies and switching times.

Measurement	*dv/dt* (V/μs)	Switching time (ns)
Turn-on with original gate circuit (SiC)	4081.9	85.5
Turn-off with original gate circuit (SiC)	3859.6	85.3
Turn-on with modified gate circuit (SiC)	5881.4	59
Turn-off with modified gate circuit (SiC)	5483.9	62
Turn-on with original gate circuit (GaN cascode)	4867.1	71.5
Turn-off with original gate circuit (GaN cascode)	4444.4	76.5
Turn-on with modified gate circuit (GaN cascode)	6123.9	56.5
Turn-off with modified gate circuit (GaN cascode)	5138.5	65

Table 3 Switching results for the different tests

5 Conclusions

In this work, an evaluation platform based on a CLLLC bidirectional resonant converter has been implemented, in order to analyse and test different technologies by simply changing the gate driver boards and the switching devices. This has made possible to run several tests, such as measurement efficiencies, influence of the gate resistors and switching times and waveforms.

The experimental results have shown that in terms of efficiency and behaviour, both SiC and GaN cascode are plausible options to develop the CLLLC converter, although the results achieved with GaN have been something better than those of SiC regarding efficiency, specially at higher frequencies. Surprisingly, as displayed in Fig. 6, for the higher gate resistor, the efficiency achieved has increased for heavier loads.

The advantage of GaN technology, namely with a cascode structure, has proven to be a faster switching time and the easier driver board, due to the absence of the negative supply rail. Its drawback is mainly the voltage rating, which happens to be too tight when the input voltage is above 600 V [19].

In a future work, the analysis and optimization of the EMI behaviour of the converter will be addressed, which will help to fulfil the EMI standards of a commercial-ready converter. This analysis will make possible to evaluate the different technologies of wide bandgap technologies in terms of electromagnetic compatibility. Also, it is possible to extend the benchmarking study to e-mode GaN HEMTs without the cascode structure, for which special driver boards have been already accomplished [20]. However, there are no GaN devices with TO-247 package of these characteristics ready in the market yet, probably due to their high parasitic inductance, and some kind of adaptation board should be carried out.

6 Reference

[1] Fahem, K., Chariag, D. E., & Sbita, L. (2017). On-board bidirectional battery chargers topologies for plug-in hybrid electric vehicles. 2017 International Conference on Green Energy Conversion Systems (GECS).

[2] Kesler, M., Kisacikoglu, M. C., & Tolbert, L. M. (2014). Vehicle-to-Grid Reactive Power Operation Using Plug-In Electric Vehicle Bidirectional Offboard Charger. IEEE Transactions on Industrial Electronics.

[3] Jian, L., Xue, H., Xu, G., Zhu, X., Zhao, D., & Shao, Z. Y. (2013). Regulated Charging of Plug-in Hybrid Electric Vehicles for Minimizing Load Variance in Household Smart Microgrid. IEEE Transactions on Industrial Electronics.

[4] Zhang, B., & Wang, S. (2020). A Survey of EMI Research in Power Electronics Systems With Wide-Bandgap Semiconductor Devices. IEEE Journal of Emerging and Selected Topics in Power Electronics.

[5] Transphorm, Inc. Characteristics of Transphorm GaN Power Switches. Application Note AN-0002.

[6] de Groot, H., Janssen, E., Pagano, R., & Schetters, K. (2007). Design of a 1-MHz LLC Resonant Converter Based on a DSP-Driven SOI Half-Bridge Power MOS Module. IEEE Transactions on Power Electronics.

[7] Dalala, Z. M., Zahid, Z. U., Saadeh, O. S., & Lai, J.-S. (2018). Modeling and Controller Design of a Bidirectional Resonant Converter Battery Charger. IEEE Access.

[8] Cree. 6.6 kW Bi-directional EV ON-BOARD CHARGER. Application Note CPWR-AN25. 2018.

[9] Texas Instruments. Designing an LLC Resonant Half-Bridge Power Converter. Power Supply Design Seminar. 2010.

[10] Zahid, Z. U., Dalala, Z., & Lai, J.-S. J. (2014). Design and control of bidirectional resonant converter for Vehicle-to-Grid (V2G) applications. In IECON 2014 - 40th Annual Conference of the IEEE Industrial Electronics Society.

[11] B. Yang, “Topology investigation of front-end dc/dc converter for distributed power system,” Ph.D. dissertation, Virginia Tech, 2003.

[12] Jung, J.-H., Kim, H.-S., Ryu, M.-H., & Baek, J.-W. (2013). Design Methodology of Bidirectional CLLC Resonant Converter for High-Frequency Isolation of DC Distribution Systems. IEEE Transactions on Power Electronics.

[13] Transphorm, Inc. Designing Hard-switched Bridges with GaN. Application Note AN-0004. 2014.

[14] Texas Instruments. Bidirectional CLLLC Resonant Dual Active Bridge (DAB) Reference Design for HEV/EV Onboard Charger. Design Guide TIDM-02002. 2019.

[15] Park, H.-P., Kim, M., & Jung, J.-H. (2020). A Comprehensive Overview in Control Algorithms for High Switching-Frequency LLC Resonant Converter. Energies.

[16] Texas Instruments. Feedback Loop Design of an LLC Resonant Power Converter. Application Report SLUA582A. 2010.

[17] Texas Instruments. C2000™ Software Frequency Response Analyzer (SFRA) Library and Compensation Designer in SDK Framework. User's Guide SPRUIK4A. 2019.

[18] Jee-hoon Jung, & Joong-gi Kwon. (2007). Theoretical analysis and optimal design of LLC resonant converter. 2007 European Conference on Power Electronics and Applications.

[19] Transphorm, Inc. Drain Voltage and Avalanche Ratings for GaN FETs. Application Note AN-0008. 2017.

[20] I. Peña, "Impacto del uso de semiconductores de banda ancha prohibida en convertidores de potencia aplicados a la movilidad eléctrica," Master Thesis, Tecnalia, 2021.